VideoCompressa: Data-Efficient Video Understanding via Joint Temporal Compression and Spatial Reconstruction

Shaobo Wang[♠]*□ Tianle Niu^{♣♠}* Runkang Yang[♠] Deshan Liu[♠] Xu He[♠]

Zichen Wen[♠] Conghui He[♠] Xuming Hu[♥] Linfeng Zhang [♠]□

EPIC Lab, SJTU [♣] KTH [♠] Shanghai AI Laboratory [♥] HKUST

* Equal contribution □ Corresponding authors

Abstract

The scalability of video understanding models is increasingly limited by the prohibitive storage and computational costs of large-scale video datasets. While data synthesis has improved data efficiency in the image domain, its extension to video remains challenging due to pervasive temporal redundancy and complex spatiotemporal dynamics. In this work, we uncover a critical insight: the primary source of inefficiency in video datasets is not inter-sample redundancy, but intra-sample frame-level redundancy. To leverage this insight, we introduce VideoCompressa, a novel framework for video data synthesis that reframes the problem as dynamic latent compression. Specifically, VideoCompressa jointly optimizes a differentiable keyframe selector—implemented as a lightweight ConvNet with Gumbel-Softmax sampling—to identify the most informative frames, and a pretrained, frozen Variational Autoencoder (VAE) to compress these frames into compact, semantically rich latent codes. These latent representations are then fed into a compression network, enabling end-to-end backpropagation. Crucially, the keyframe selector and synthetic latent codes are co-optimized to maximize retention of task-relevant information. Experiments show that our method achieves unprecedented data efficiency: on UCF101 with ConvNets, VideoCompressa surpasses fulldata training by 2.34% points using only 0.13% of the original data, with over 5800× speedup compared to traditional synthesis method. Moreover, when fine-tuning Qwen2.5-7B-VL on HMDB51, VideoCompressa matches full-data performance using just 0.41% of the training data—outperforming zero-shot baseline by 10.61%.

1. Introduction

Recent advances in vision-language models (VLMs) have been largely driven by the availability of large-scale vision datasets [1, 2, 23, 51, 63]. However, as the data grows exponentially, the training and storage costs as-

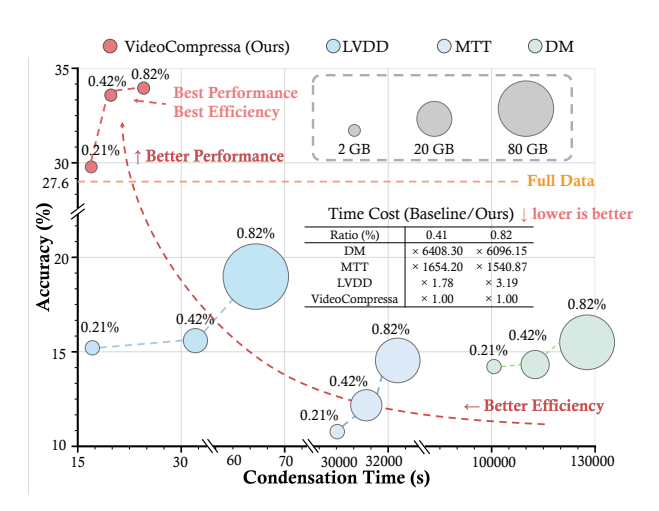


Figure 1. Comparison of performance and computation efficiency across different compressing methods under multiple compression ratios on UCF101 dataset. Bubble size indicates peak GPU memory usage during compression. VideoCompressa achieves substantially better performance with dramatically lower computation cost, reaching over 5800× speedup compared to prior compression methods such as DM, MTT, and LVDD. The dashed orange line marks full-data supervised training.

sociated with such datasets have become major bottlenecks [12, 48, 58, 69]. This data-scaling challenge has motivated a growing field of research focused on data-efficient learning [24, 44, 46]. A highly promising solution is dataset compression, which has achieved tremendous success in the image domain [8, 9, 28, 37, 43, 49, 54–57, 64, 70]. However, translating this success to the video domain is non-trivial and presents unique challenges [42, 45, 53]. First, videos introduce a temporal dimension, which is rife with redundancy, adjacent frames are often nearly identical, naively compressing all frames is computationally infeasible and informationally wasteful [19, 33, 66]. Second, the sheer scale of video data makes many pixel-space optimization methods, common in image distillation, intractable [11, 59, 71]. Third, the complex spatiotemporal dynamics that define an action may be subtle and occur in short bursts, making simple heuristic-based frame selection highly suboptimal [14, 21, 23]. Despite the prevalence of keyframe selection [13, 38, 62] as a technique for efficient video processing in large multimodal models [18, 50, 65], its potential for the task of large-scale video action dataset compression still remains unexplored.

Prior attempts at video dataset compression also have several limitations. Coreset selection methods [10, 16, 27, 39] simply select a subset of real videos, which is storage-inefficient and fails to create a densified representation. Pixel-space compression methods like VDSD [59] and DATM [11] attempt to synthesize video pixels, but struggle with the high computational cost, limiting their scalability and compression ratios. Though IDTD [71] jointly considers the unique within-sample and inter-sample redundancies of video, it still struggles to capture sufficient information diversity at low sample settings. More recently LVDD [30] explored latent space compression, but it typically decouple temporal selection from the latent optimization process, which limits its flexibility and generalization.

To this end, we propose VideoCompressa, a framework that for the first time, jointly learns to select salient keyframes and synthetize a compact latent video dataset in an end-to-end manner. Our approach tackles temporal and spatial redundancy simultaneously. Instead of relying on fixed heuristics or decoupled pipelines [30], we treat both the keyframe selection and the synthetic data content as learnable parameters of a single, unified compression objective. Our method is built on three key ideas. First, we move the compression process from the high-dimensional pixel space to the compact latent space through a lightweight pretrained VAE encoder [6]. Second, instead of using a fixed temporal sampling heuristic, we introduce a differentiable keyframe selection module powered by the Gumbel-Softmax reparameterization [20, 22, 40] to selects the most salient Kframes for visual understanding. Third, we jointly optimize the synthetic latent codes and the parameters of the keyframe selection network. Extensive experiments show our method achieves new state-of-the-art results, dramatically outperforming existing methods on large-scale benchmarks (as shown in Figure 1) and achieving lossless compression on UCF101 dataset. Critically, we demonstrate that our highly compressed datasets can also be used to fine-tune Multimodal Large Language Model (MLLM), achieving performance remarkably close to models fine-tuned on the entire dataset. Contributions are summarized as follows:

- We identify intra-sample frame-level redundancy, rather than inter-sample redundancy, as the principal source of inefficiency in large-scale video datasets. We argue that effective data compression must therefore prioritize principled temporal information selection over uniform sequence compression.
- 2. To act on this insight, we introduce *VideoCompressa*,

- a novel end-to-end framework for video data compression. Our method uniquely co-optimizes a differentiable Gumbel-Softmax keyframe selector with the reconstruction of compact latent codes, ensuring that both *which* frames to select and *how* to represent their content are jointly guided by the task objective.
- 3. We demonstrate state-of-the-art performance and unprecedented data efficiency, achieving a state of lossless data compression on several datasets. For standard ConvNets on UCF101, our method surpasses full-data performance by 2.34% using merely 0.13% of the original data. This remarkable efficiency generalizes to modern architectures; when fine-tuning a MLLM on HMDB51, our method matches full-data performance using just 0.41% of the data.

2. Related Work

Key-Frame Selection for Video Understanding. Keyframe selection is a cornerstone of efficient video understanding [3, 13, 38, 62, 65]. The field has progressed from fast but rigid heuristics (e.g., uniform sampling, pixel differences) [3, 32, 68] to more sophisticated, differentiable schemes that learn to select frames based on task relevance and temporal coverage [50]. However, the primary application of these advanced selection methods has been to accelerate inference on pre-trained models [5, 32, 68]. Their potential for creating a synthetic dataset from scratch—as a core component of the data generation process itself—remains largely unexplored. Our work bridges this gap by directly integrating a differentiable key-frame selection mechanism into the dataset synthesis pipeline. This novel approach enables, for the first time, the joint optimization of which frames to select and how to represent their content, tackling both temporal and spatial redundancy in a unified framework.

Efficient Dataset Synthesis. The quest for data efficiency has spurred the development of powerful dataset compression techniques, which create compact data surrogates that retain the performance of the full dataset, primarily in the image or language domain [28, 43, 49, 54, 57, 67]. Extending this paradigm to video is complicated by immense temporal redundancy [19, 26, 34, 35, 45, 53]. Early videocentric approaches like VDSD [59] and DATM [11] attempt to synthesize video pixels directly. While VDSD disentangles static and dynamic content, both methods grapple with the high computational cost and scalability issues inherent to pixel-space optimization, without explicitly learning which frames are most informative. To mitigate this, recent work like LVDD [30] has moved the synthesis process into a more efficient latent space. However, it relies on fixed, selection-centric heuristics rather than a learnable optimization process, limiting its flexibility and the quality of the resulting summary. Consequently, a critical gap remains:

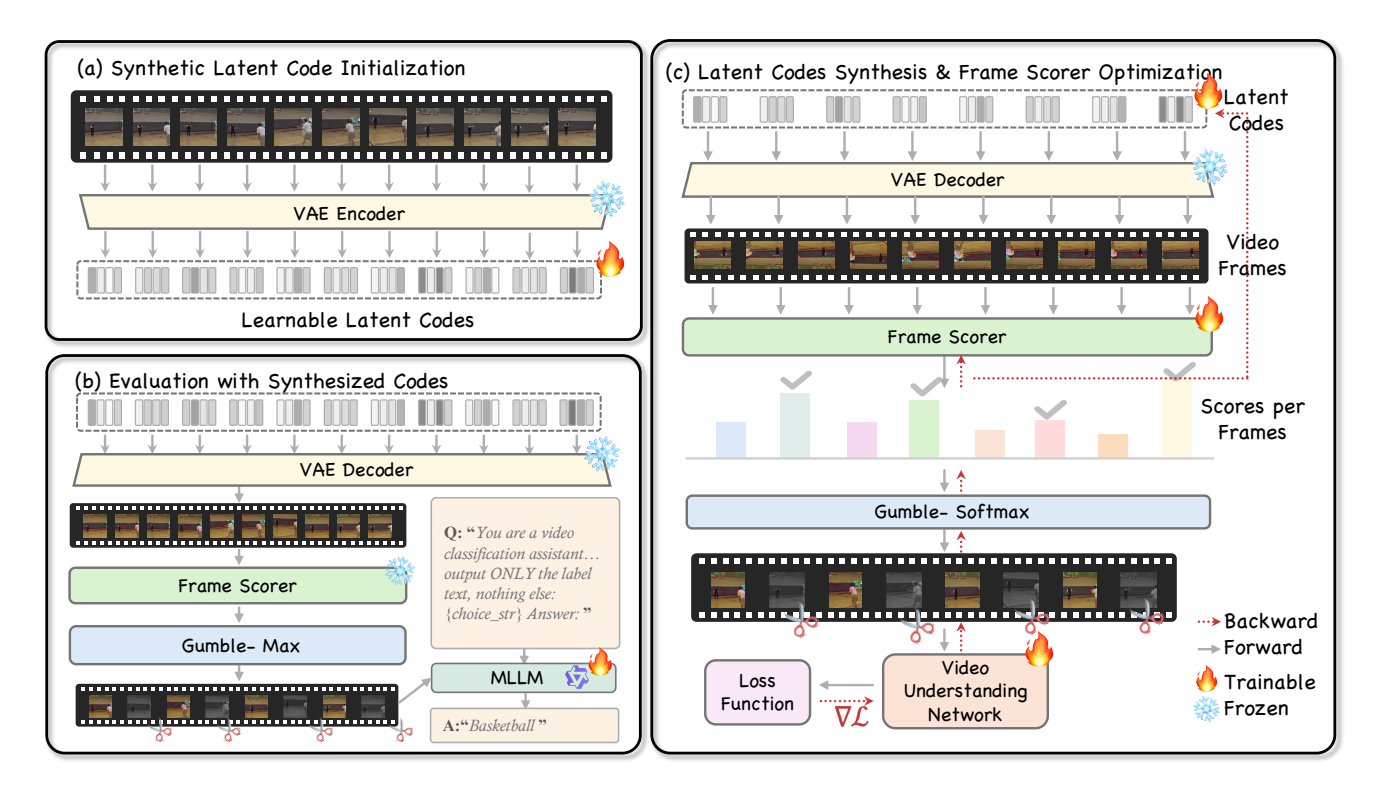


Figure 2. An overview of our proposed pipeline. A raw video is first processed by a Gumbel-based keyframe selection module. The selected keyframes are then encoded into the latent space by a frozen VAE. Finally, these latent representations are optimized via latent space synthesis, guided by the gradients from a student model, to form the synthetic dataset.

current methods condense video sequences but fall short of strategically selecting the most salient temporal information, leaving a rich source of efficiency untapped.

3. Preliminary: Data-Efficient Video Under- standing

Given a video training dataset $\mathcal{D}_{\text{train}} = \{(\mathcal{V},y)\}_{i=1}^N$, where $N = |\mathcal{D}_{\text{train}}|$ and each $\mathcal{V} = \{f_{i,t}\}_{t=1}^T$ is a sequence of T frames, and a held-out test set $\mathcal{D}_{\text{test}}$ sampled from the same distribution, the goal of *data-efficient video understanding* is to construct a compact, compressed representation \mathcal{S} of $\mathcal{D}_{\text{train}}$ that preserves its discriminative power for video understanding tasks. This is achieved by designing an algorithm \mathcal{A} that transforms $\mathcal{D}_{\text{train}}$ into a compact dataset $\mathcal{S} = \mathcal{A}(\mathcal{D}_{\text{train}})$ with size $M = |\mathcal{S}| \ll N$. Mathematically, we formalize this objective as follows:

Definition 1 (Data-Efficient Video Understanding). Let $\mathcal{M}(\cdot)$ denote a learning algorithm that maps a dataset to a model, and let \mathfrak{M} be a class of admissible learning algorithms. Given a fixed compressed dataset size $M \ll N$, the goal is to design an algorithm \mathcal{A} that produces $\mathcal{S} = \mathcal{A}(\mathcal{D}_{\text{train}})$ with $|\mathcal{S}| = M$, such that the worst-case performance gap on

the test set is bounded:

$$\sup_{\mathcal{M} \in \mathfrak{M}} |\mathcal{L}(\mathcal{M}(\mathcal{S}); \mathcal{D}_{test}) - \mathcal{L}(\mathcal{M}(\mathcal{D}_{train}); \mathcal{D}_{test})| \le \delta(M),$$
(1)

where $\mathcal{L}(f;\mathcal{D}_{\mathrm{test}}) = \mathbb{E}_{(\mathcal{V},y) \sim \mathcal{D}_{\mathrm{test}}}[\ell(f(\mathcal{V}),y)]$ is the expected test loss and $\delta(M) \geq 0$ is a tolerance that depends on M. The objective is to minimize $\delta(M)$ for a given M.

4. Methodology

We propose *VideoCompressa*, a unified framework for data-efficient video understanding that jointly optimizes temporal compression and spatial reconstruction. As illustrated in Figure 2, our approach processes each input video $\mathcal V$ through two co-optimized stages: (1) *Gumbel-based temporal compression* that dynamically selects a minimal set of informative frames, and (2) *latent spatial reconstruction* that refines visual content in the VAE latent space. Crucially, both stages are differentiable and jointly trained with the downstream video understanding network, enabling end-to-end optimization of the compressed representation $\mathcal S$ under the data-efficiency constraint $|\mathcal S|=M$. The entire pipeline is trained to minimize the performance gap $\delta(M)$ defined in Section 3.

Latent Code Initialization. Before optimization, each video $\mathcal{V} = \{f_t\}_{t=1}^T$ is encoded into an initial latent representation

using a pre-trained VAE with an encoder $\mathcal E$ and a decoder ψ . Specifically, we apply the VAE encoder $\mathcal E$ to each frame to obtain latent codes $\mathbf z_t = \mathcal E(f_t) \in \mathbb R^d$, forming the initial latent sequence $\mathbf Z = \{\mathbf z_t\}_{t=1}^T$. These latent codes serve as (i) the basis for decoding pixel frames via ψ that feed into temporal compression, and (ii) optimization variables for spatial reconstruction.

4.1. Gumbel-Based Temporal Compression

We first perform temporal compression to select key-frames within each video. This is achived by training a *frame scorer* via Gumbel-Softmax technique. The frame selector operates on decoded pixel frames to capture visual semantics. For each input latent code $\mathbf{Z} = \{\mathbf{z}_t\}_{t=1}^T$, we first obtain the decoded frame sequence $\hat{\mathcal{V}} = \{\hat{f}_t\}_{t=1}^T$, where $\hat{f}_t = \psi(\mathbf{z}_t)$ and ψ is the frozen VAE decoder.

Specifically, a lightweight neural network ϕ , composed of two 2D convolutional layers followed by a linear layer, is used as the frame scorer. It processes the entire decoded sequence to produce a score vector $\mathbf{q} \in \mathbb{R}^T$, i.e., $\mathbf{q} = \phi(\hat{f}_1, \dots, \hat{f}_T)$, where each element q_t represents the importance score of frame t. These logits are normalized via softmax to form selection probabilities:

$$p_t = \frac{\exp(q_t)}{\sum_{t'=1}^{T} \exp(q_{t'})}.$$
 (2)

To enable differentiable selection of K frames ($K \ll T$), we apply the Gumbel-Softmax reparameterization [22] with temperature $\tau = 1$. For each of K independent samples $k = 1, \ldots, K$, we draw Gumbel noise per frame:

$$g_t^{(k)} = -\log(-\log(u_t^{(k)})), \quad u_t^{(k)} \sim \text{Uniform}(0,1), \quad (3)$$

and compute a soft selection distribution:

$$\tilde{p}_t^{(k)} = \frac{\exp\left((q_t + g_t^{(k)})/\tau\right)}{\sum_{t'=1}^T \exp\left((q_{t'} + g_{t'}^{(k)})/\tau\right)}.$$
 (4)

Each sample yields one expected frame via soft aggregation:

$$\hat{f}^{(k)} = \sum_{t=1}^{T} \tilde{p}_t^{(k)} \cdot \hat{f}_t.$$
 (5)

The final compressed video is formed by concatenating the K selected frames:

$$\tilde{\mathcal{V}} = \left[\hat{f}^{(1)}, \hat{f}^{(2)}, \dots, \hat{f}^{(K)} \right].$$
 (6)

Gradient Propagation via Gumbel-Softmax. Gradients from the classification loss flow through each $\hat{f}^{(k)}$ via the Gumbel-Softmax path. The gradient w.r.t. the logits \mathbf{q} is approximated by averaging over K samples:

$$\nabla_{\mathbf{q}} \mathcal{L} \approx \frac{1}{K} \sum_{k=1}^{K} \nabla_{\tilde{\mathbf{p}}^{(k)}} \mathcal{L} \cdot \nabla_{\mathbf{q}} \tilde{\mathbf{p}}^{(k)}, \tag{7}$$

where $\nabla_{\mathbf{q}}\tilde{\mathbf{p}}^{(k)}$ follows from the softmax Jacobian. Since ϕ operates on decoded frames and ψ is frozen, gradients update only the parameters of ϕ .

Downstream Inference. At inference, we perform deterministic top-K selection: we select the K frames with highest logits \mathbf{q} to form $\tilde{\mathcal{V}} = \{\hat{f}_t\}_{t \in \mathcal{T}_K}$, where $\mathcal{T}_K = \text{top-}K(\mathbf{q})$. This yields a compact representation with exactly K frames, ensuring minimal computational overhead.

4.2. Latent Spatial Reconstruction

Following temporal compression, we optimize the latent codes of the selected frames rather than pixel-level representations to minimize storage overhead. Storing optimized latents requires significantly less space than full-resolution frames while preserving discriminative features. These latent codes are jointly updated with the video understanding model through end-to-end classification training. We optimize three components simultaneously: the latent codes \mathbf{Z} , the temporal scorer ϕ , and the video understanding model \mathcal{M}_{θ} . The objective is defined as:

$$\underset{\mathbf{Z},\phi,\theta}{\operatorname{arg\,min}} \sum_{i=1}^{N} \mathcal{L}_{CE} \left(\mathcal{M}_{\theta} \left(\tilde{\mathcal{V}}(\mathbf{Z},\phi) \right), y \right), \tag{8}$$

where $\tilde{\mathcal{V}}$ is the temporally compressed video constructed as in Section 4.1. This single-objective formulation creates a closed optimization loop:

- 1. \mathcal{M}_{θ} learns features from compressed videos under supervision of original hard labels y
- 2. ϕ adapts frame selection to maximize classification accuracy (via gradients through $\tilde{\mathcal{V}}$)
- 3. **Z** are refined through gradients flowing backward through ψ and \mathcal{M}_{θ}

Although the temporal scorer operates on decoded frames, gradients from the classification loss \mathcal{L}_{CE} propagate through $\tilde{\mathcal{V}}$ to the latent codes \mathbf{Z} via the frozen decoder ψ . Specifically, for each latent code \mathbf{z}_t , the gradient $\partial \mathcal{L}_{\text{CE}}/\partial \mathbf{z}_t$ adjusts its representation to improve classification performance. Crucially, no auxiliary losses or regularization terms are introduced—all optimization is driven solely by the classification signal. This ensures spatial reconstruction is strictly task-oriented, while the fixed frame budget k inherently enforces temporal compression. The co-optimization directly minimizes the performance gap $\delta(M)$ from Definition 1 through end-to-end training.

5. Experiments

5.1. Experimental Setup

Datasets. We adopted medium-scale video datasets UCF101 [47] and HMDB51 [25], as well as large-scale video datasets Kinetics-400 [7] and Something-Something-V2 (SSv2) [15] in our experiments. UCF101 [47] consists

Table 1. Classification accuracy (%) for data condensation on different video dataset synthesis benchmarks under different ratio settings. All methods use a randomly initialized ConvNet and FrameScore network to guide synthesis, with accuracy measured by training that same ConvNet from scratch on the resulting condensed data.

Dataset	Ratio (%)	Coreset Selection			Data Synthesis					Full Data			
		Random	Herding	Forgetting	GraNd	DM+VDSD	MTT+VDSD	MTT	DM	DATM	LVDD	VideoCompressa	Full Data
HMDB51	0.21	13.49±0.08	17.26±0.51	18.82±0.24	17.30±0.48	7.20±0.32	6.94±0.11	5.99±0.33	6.29±0.10	10.01±0.36	7.78±0.29	27.78±1.14	Ī
	0.41	13.56±0.32	16.16±0.99	19.60±0.24	16.58±0.39	6.99±0.10	7.03±0.29	6.11±0.42	6.32±0.22	10.02±0.41	11.60±0.30	28.00±0.45	28.08±0.89
	0.82	13.69±0.37	15.84±0.69	18.93±0.48	16.71±0.48	8.13±0.23	8.77±0.34	9.34±0.31	8.97±0.11	13.77±0.33	15.35 ± 0.26	28.51±0.07	
	0.13	17.76±1.15	13.80±0.33	13.65±0.04	13.45±0.11	14.72±0.46	13.99±0.28	10.76±0.32	9.58±0.09	11.89±0.63	15.32±0.61	29.84±0.75	ī
UCF101	0.26	17.62±0.76	13.59±0.34	14.02±0.38	13.71±0.11	13.98±0.39	14.44±0.53	11.11±0.10	9.61±0.31	12.14±0.62	16.47±0.44	34.28±0.61	27.60±0.62
	0.52	18.31±0.82	13.46±0.26	13.61±0.10	14.04 ± 0.45	14.78±0.43	18.84±0.54	14.56±0.19	12.11±0.24	14.33±0.76	19.99±0.42	34.03±0.27	
SSv2	0.72	1.26±0.10	1.12±0.16	1.95±0.21	2.12±0.32	4.04±0.22	4.11±0.63	5.01±0.59	3.69±0.26	5.10±0.22	4.31±0.77	8.18±0.33	<u> </u>
	1.45	2.07±0.11	3.18±0.33	4.17±0.32	3.94±0.51	4.10±0.35	5.99±0.50	5.12±0.46	4.01±0.11	5.02±0.48	5.99±0.22	18.82 ± 0.60	24.07±0.50
	2.90	3.39±0.32	4.31±0.12	5.17±0.40	4.63±0.33	5.01±0.20	7.92±0.29	6.68±0.33	4.42±0.49	5.97±0.69	8.03±0.45	23.97±0.71	
Kinetics-400	0.04	1.14±0.13	1.23±0.11	1.79±0.50	2.01±0.39	4.82±0.05	4.71±0.09	3.44±0.02	3.04±0.33	4.78±0.33	4.48±0.75	9.96±0.59	I
	0.09	3.33±0.20	3.07±0.44	4.24±0.48	4.38±0.44	5.45±0.33	4.44±0.23	3.42±0.11	3.03±0.57	5.32±0.31	6.67±0.21	16.77±0.71	29.77±0.54
	0.17	3.78±0.21	4.14±0.32	4.95±0.63	4.71±0.57	7.02±0.16	8.40±0.53	7.61±0.38	7.79 ± 0.82	7.96±0.46	10.99±0.13	19.97±0.66	

of 13,320 video clips spanning 101 action categories, while HMDB51 [25] includes 6849 video clips from 51 action categories. Kinetics-400 [7] comprises a diverse collection of videos covering 400 human action classes, whereas SSv2 focuses on 174 motion-centric classes with subtle temporal dynamics. We followed previous works to report the top-1 classification accuracy for UCF101 and HMDB51, and the top-5 classification accuracy for Kinetics-400 and SSv2.

Baselines. We compared our method against two categories of baselines: (i) *selection-based* compression and (ii) *synthesis-based* compression. For selection-based compression, which selects a representative subset of real videos, we included four algorithms: Random, Herding [61], Forgetting [52], and GraNd [41]. For synthesis-based method, which synthesizes a new, compact dataset, we benchmarked against several state-of-the-art approaches: DM [70], MTT [8], DATM [17], and LVDD [31]. To ensure a comprehensive evaluation against the latest advancements, we also integrated the static-dynamic disentanglement strategy from the recent VDSD [60] with established methods. We also reported results for these hybrid baselines, DM+VDSD and MTT+VDSD, to thoroughly assess the efficacy of different compression strategies.

Models. We employed a lightweight 2-layer 2D-CNN with a single linear layer as the frame scorer $f_{\rm scorer}$, and a 3-layer 2D-CNN for video understanding. The VAE model is implemented using the pre-trained TAESD [6] model, a compact 2D VAE model that occupies only 9MB. For convolutional network experiments, we used the same 2D-CNN for evaluation. For MLLM experiments, we utilized the Qwen2.5-VL-7B [4] model for evaluation.

Implementation Details. All experiments were conducted on 8 NVIDIA A100 GPUs. For the latent code reconstruction, we used the Adam optimizer to update the synthetic latent codes ${\bf Z}$ and the scorer ϕ . The learning rate was set to 1×10^{-2} for the latent code and 1×10^{-3} for the scorer. To ensure fairness, all experiments were conducted for 3 times. More details are included in Appendix.

Table 2. Cross-architecture accuracy (%) on the UCF101 dataset with a 0.13% data budget. A random initialized ConvNet model is used to guide the iteration of synthetic datasets, which are then evaluated by training different architectures from scratch.

Method	Classification Network ConvNet MLP RNN GRU						
Random	16.66+0.34	1.07+0.16	1.15±0.10	1.02±0.29			
Forgetting	7.31±0.30	1.25 ± 0.12	1.24 ± 0.16	0.85 ± 0.17			
Herding	11.45±0.35	1.04 ± 0.08	1.05 ± 0.12	1.31 ± 0.21			
LVDD	15.32±0.61	15.45 ± 0.15	$13.92{\scriptstyle\pm0.52}$	14.44 ± 0.72			
VideoCompressa	29.84 ± 0.75	$23.97{\scriptstyle\pm0.53}$	$26.07{\scriptstyle\pm0.57}$	$26.15{\scriptstyle\pm0.32}$			
Full Data	27.60±0.62	24.87±0.46	25.15±0.33	26.99±0.71			

5.2. Results on Convolutional Networks

Comparison with Baselines. As shown in Table 1, Video-Compressa approach significantly outperforms all competing methods across all datasets and settings. Specifically, VideoCompressa surpasses all other methods in classification accuracy on the HMDB51, UCF101, Kinetics-400, and SSv2 datasets for all data compression ratios. A particularly compelling result is that *our VideoCompressa achieves better performance with training on the full data of HMDB51 and UCF101, requiring only 0.82% and 0.13% of the respective entire datasets*.

Cross-Architecture Performance. We conducted a rigorous cross-architecture generalization experiment, with results presented in Table 2. Following a standard protocol, we used a randomly initialized ConvNet to guide the reconstruction process. Subsequently, we used the resulting synthetic latent code to generate decoded synthetic dataset. The dataset is used to train a variety of architectures from scratch: a ConvNet, an MLP, an RNN, and a GRU. The results unequivocally demonstrate the superior generalization of the dataset synthesized by VideoCompressa. Our method consistently outperforms all competing approaches across every target architecture, highlighting that synthetic data is not overfitted to the guiding ConvNet but has instead captured more fundamental and transferable data characteristics. The performance gap is substantial; when compared to

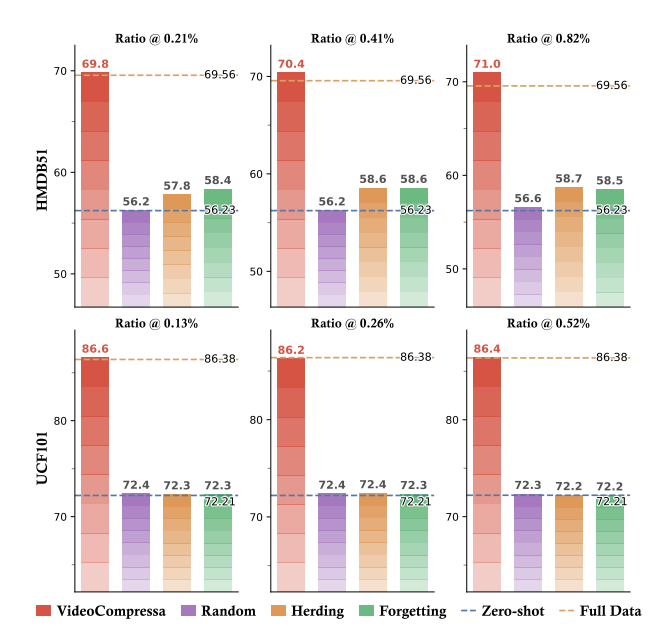


Figure 3. Classification accuracy (%) for data compression on HMDB51 and UCF101 video benchmarks under different ratio settings. All methods use a randomly initialized ConvNet and frame scorer to guide reconstruction, with accuracy measured by finetuning pre-trained Qwen2.5-VL-7B from scratch on the resulting condensed data.

the strongest baseline for each model family, our approach achieves absolute accuracy gains of +13.18% on ConvNet, +8.52% on MLP, +12.15% on RNN, and +11.71% on GRU. Computational Efficiency Analysis. We further analyzed the computational efficiency of different synthesis-based methods in terms of both compression time and GPU memory usage, as summarized in Figure 1. Compared to previous baselines such as DC, DM, and MTT, VideoCompressa achieves a remarkable reduction in resource consumption while maintaining superior accuracy. Specifically, at a 0.52% compression ratio on UCF101, our method runs over 5800× faster than DC, requiring only 20.5 seconds for compression, and consumes merely 24.8 GB of GPU memory—saving up to 45 GB compared to existing approaches. Despite its lightweight cost, VideoCompressa surpasses full-data training by 5.43% in classification accuracy. These results highlight the scalability and efficiency of our approach for large-scale video dataset reconstruction.

5.3. Results on Multimodal Large Language Models

The proposed VideoCompressa framework generalizes effectively to MLLMs, demonstrating strong compression capability and transferability across architectures. As illustrated in Figure 3, our method achieves *lossless compression on MLLM*, surpassing full-dataset Supervised Fine-Tuning (SFT) on both HMDB51 and UCF101 while using merely 0.21% and 0.13% of the original training data, respectively. This remarkable result indicates that our distilled data pre-

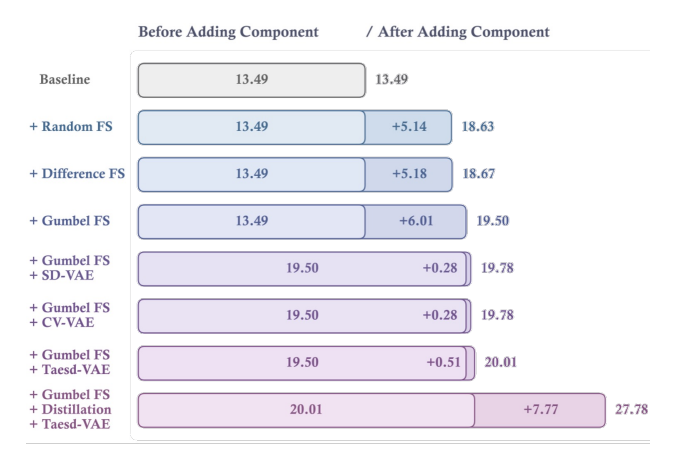


Figure 4. Ablation study of individual components. The figure compares the impact of three Frame Selection methods, three VAE variants, and the inclusion of the video understanding module. Experiments are conducted on UCF101 with a 0.13% data ratio. FS indicates frame selection method.

Table 3. Performance of different key-frame selection strategies on the HMDB51 dataset. To isolate the impact of the selection method itself, the understanding network was disabled, and each strategy selected a fixed budget of 4 frames. Our learnable Gumbel-Max approach significantly outperforms both the no-selection baseline and common heuristic methods.

Selection Method	l None	Uniform	Pixel Diff.	Gumbel-Max (Ours)
Accuracy	13.49±0.08	18.63 ± 0.43	$18.67{\scriptstyle\pm0.78}$	19.50±0.82

serve both semantic and temporal richness essential for multimodal understanding. Compared to the previous state-of-theart baseline, *VideoCompressa achieves an 11.4% absolute improvement on HMDB51 and an 8.2% gain on UCF101*, establishing a new performance upper bound under extreme data reduction. These results highlight that our approach not only compresses large-scale video datasets efficiently but also enhances generalization for MLLM-based video understanding tasks.

5.4. Ablation Study

We conducted a comprehensive ablation study to meticulously evaluate the contribution of each component within our VideoCompressa framework. The results are illustrated in Figure 4. Our analysis follows a cumulative design, starting from a random baseline that achieves 13.49% accuracy. First, we integrated and compared three different key-frame selection methods. Among them, Gumbel-Max frame selection method provides the most significant improvement, boosting the accuracy by 6.01% to 19.50%. Building upon this enhanced model, we then evaluated three VAE variants, where the Taesd-VAE proved most effective, further increasing the accuracy to 20.01%. Finally, the inclusion of our reconstruction process yields a substantial gain of 7.77%, bringing the final accuracy to 27.78%.

Table 4. Impact of different VAE architectures on classification accuracy (%) and computational efficiency on the HMDB51 dataset. To isolate the VAE's contribution, accuracy was evaluated with the synthesis component disabled. Computational efficiency was measured during a single iteration step. For a fair comparison, all configurations select 4 frames using the Gumbel-Max strategy. OOM indicates out-of-memory.

VAE Type VAE Size (MB)	No VAE	SD-VAE 335	CV-VAE 80	Taesd-VAE 9
Accuracy ↑	19.50	19.78	19.78	20.01
GPU Memory (GB) ↓	>800	25.13	24.82	24.80
Time (s) \downarrow	OOM	388.62	57.15	22.86

Impact of Key-Frame Selection Strategies. We dissect the contribution of the key-frame selection module by conducting an ablation study in a decoupled setting. To strictly isolate the impact of the selection mechanism, we trained the models from scratch using a fixed budget of 4 frames selected by each strategy. We compared our approach against two common heuristics: Uniform Sampling and Pixel Differencebased Selection. As detailed in Table 3, the introduction of any structured key-frame selection strategy yields a substantial performance leap over the baseline, confirming that reducing temporal redundancy is critical for data efficiency. Most importantly, our Gumbel-Max strategy achieves the highest accuracy of 19.50%, surpassing both uniform and difference-based heuristics. It is worth noting that in this setting, the Gumbel selector operates without the supervisory gradients from the training process. The fact that it outperforms handcrafted heuristics even in this decoupled regime validates its intrinsic ability to adaptively identify the most information-rich temporal segments for the task.

Impact of VAE on Computational Efficiency. To quantify the efficiency gains brought by different VAE designs, we conducted an ablation that replaces the VAE architecture while keeping the rest of the pipeline fixed. As shown in Table 4, Taesd-VAE significantly improves computational efficiency while preserving accuracy. By compressing videos into a compact latent space, VAE-based methods reduce the input dimensionality and yield at least ×32 reduction in memory consumption. In particular, Taesd-VAE achieves ×17 speedup over SD-VAE, making it the most efficient choice without sacrificing performance.

Ablation on coupled effect of the Understanding Network and Gumbel Trick. To isolate the contribution of the video understanding network, we evaluated Uniform and Gumbel-Max key-frame selection strategies on HMDB51 under varying numbers of training steps. As shown in Table 5, the Gumbel Trick frame selector benefits substantially from the presence of the supervisory gradients from the video understanding network, since its parameters are updated through the Gumbel-Softmax. *Notably, Gumbel Trick achieves a 7.91% accuracy gain at 4 steps*, highlighting the

Table 5. Classification accuracy (%) on HMDB51 under 2 different frame selection methods. For a fair comparison, all experiments were conducted under a fixed setting that selects 4 frames.

Training Step	Uniform	Gumbel Trick (Ours)
0	18.63±0.43	19.50 ± 0.82
1	18.31±0.92	$26.27{\scriptstyle\pm0.38}$
2	18.53±1.09	26.47 ± 0.46
4	19.87±0.39	27.78 ± 1.14

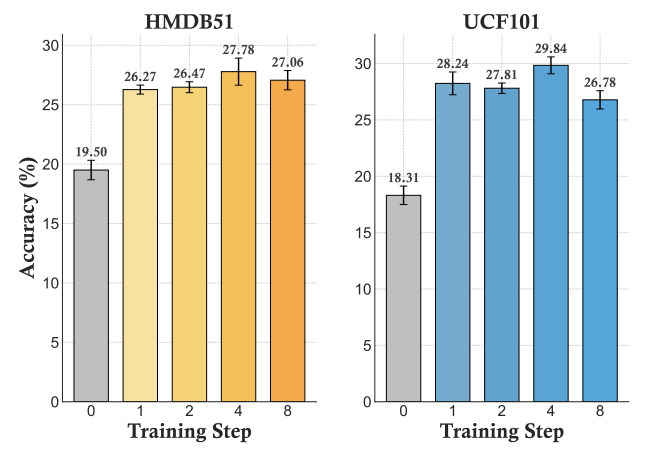


Figure 5. Sensitivity analysis of training steps on HMDB51 and UCF101. All experiments were conducted under a fixed setting: selecting 4 frames with the Gumbel-based strategy.

strong coupling between the frame selection network and the understanding component. This further confirms the feasibility of exploiting intra-sample redundancy for video compression and underscores the effectiveness of our proposed framework.

Sensitivity analysis of reconstruction steps. To assess the robustness of our approach, we performed a sensitivity analysis on both HMDB51 and UCF101. As illustrated in Figure 5, VideoCompressa maintains consistently strong performance across different training steps, demonstrating stable behavior under varying training dynamics.

6. Discussion

6.1. Why Prior Methods Fall Short: Intra-Sample Redundancy Must Be Prioritized Over Inter-Sample Redundancy

A critical analysis of prior video dataset compression techniques reveals a fundamental limitation: an overemphasis on resolving *inter-sample* redundancy while largely neglecting the far more significant issue of *intra-sample* redundancy. Many previous approaches, such as coreset selection [41, 52, 61], treat each video as an indivisible atomic unit, thereby failing to address the massive data repetition that exists *within* each sample. This oversight is the principal reason for their suboptimal performance. As shown in

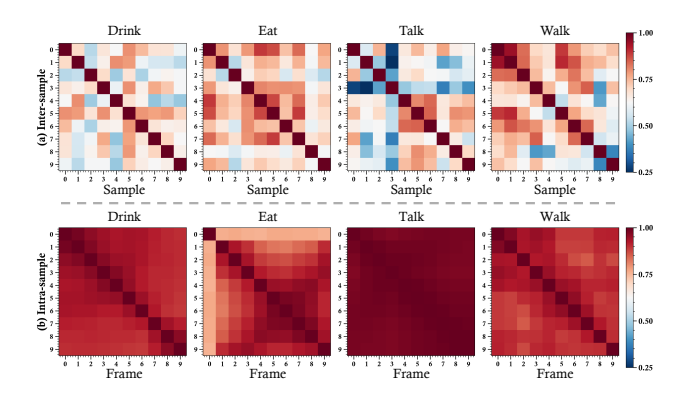


Figure 6. Visualization of inter-sample versus intra-sample redundancy for select action classes from the UCF101 dataset.

Figure 6, The core inefficiency of large-scale video datasets stems not from the similarity between different videos, but from the high temporal correlation between consecutive frames in a single video. The inter-sample correlation matrices show that while videos of the same class are related, there is considerable variance between them, indicated by the mix of high and low correlation values off the main diagonal. Simply discarding entire videos risks losing the diverse expressions of an action. In stark contrast, the intra-sample matrices demonstrate overwhelmingly high correlation between adjacent frames. The deep red coloring across these heatmaps signifies pervasive redundancy, where consecutive frames often contain nearly identical information. Methods that focus only on inter-sample compression are forced to retain all of this redundant data for any video they select. Consequently, they fail to create a truly dense and efficient data representation. Our work posits that a paradigm shift is necessary: effective video data compression must prioritize the principled selection of informative temporal segments within each video, directly tackling the primary source of data inefficiency.

6.2. Why Differentiable Frame Selection Works Well: Dynamic Compression Matters

To elucidate the working principles behind the effectiveness of key-frame selection in video datasets, we conducted a comparative analysis of selection-based and synthesis-based methodologies. This investigation was performed on the UCF101 dataset, employing a sampling ratio of 0.13%. We utilized the Uniform Manifold Approximation and Projection (UMAP) [36] technique for dimensionality reduction, enabling a 2D visualization of the feature space to assess the data distribution. As illustrated in Figure 7, the distribution produced by our method, VideoCompressa, most closely mirrors the ground-truth data distribution. This indicates that VideoCompressa achieves a superior trade-off between representativeness and diversity, which we identify as the key principle for its success. For instance, within the UnevenBars

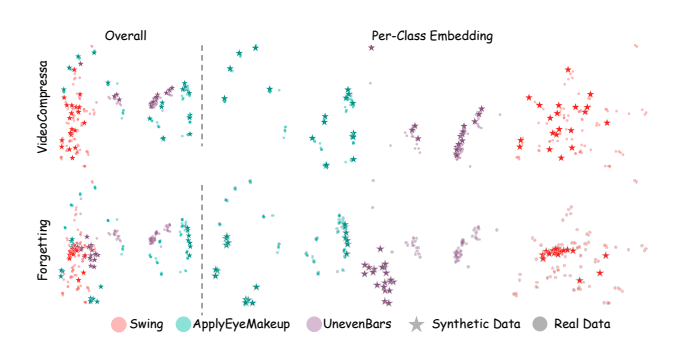


Figure 7. UMAP visualization comparing the feature distributions of real data and synthetic data on the UCF101 dataset.

category, VideoCompressa's synthesized data points are densely clustered around the distribution's center, effectively capturing the core characteristics of this class. In contrast, the Forgetting method fails to adequately represent this central region. Furthermore, in the ApplyEyeMakeup category, the embedding generated by VideoCompressa demonstrates significant diversity. The visualization reveals multiple distinct clusters with substantial inter-cluster distances—a topological feature adeptly captured by VideoCompressa but overlooked by the Forgetting method. This observation corroborates previous findings [29] which suggest that preserving diversity is a critical factor in the performance of dataset synthesis tasks for image-based datasets.

7. Qualitative Analysis

To rigorously evaluate the effectiveness of VideoCompressa in capturing complex temporal dynamics, we provide a qualitative visualization on the Something-Something V2 (SSv2) dataset. Unlike static image datasets, SSv2 relies heavily on temporal ordering and causal reasoning, making it an ideal testbed for verifying our differentiable keyframe selection mechanism. Figure 8 presents a comprehensive comparison between 16 frames uniformly sampled from the original video, a standard random selection baseline, and the 4-frame sequence reconstructed from our compressed latent codes. **Superior Temporal Selection.** As evidenced by the com-

Superior Temporal Selection. As evidenced by the comparison, Uniform Sampling often misses critical transition states due to its rigid interval selection, as clearly shown in the "Uniform Selection" column. In contrast, our Gumbelbased selector demonstrates intelligent budget allocation prioritized by semantics. Specifically, for the action "Poking [something] so that it falls over" in the first row, our model explicitly selects the exact moment the object loses balance in the third frame, whereas Uniform Sampling captures only the static pre- and post-action states, effectively severing the causal link of the object's disappearance. Furthermore, in the "Pouring [something] onto [something]" example presented in the fourth row, our method retains the frame exhibiting the stained surface—visual evidence of the action's consequence

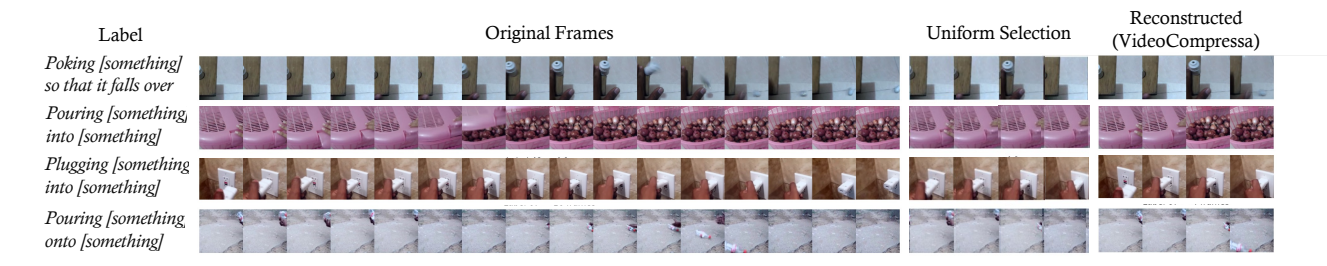


Figure 8. Qualitative comparison of temporal compression on Something-Something V2. The figure contrasts 16 uniformly sampled original frames on the left against 4-frame sequences obtained via Uniform Sampling in the middle and our VideoCompressa reconstruction on the right. While Uniform Sampling often yields static snapshots due to rigid striding, our method prioritizes semantically critical moments. For instance, our model captures the causal transition of an object tipping over in the first row and the visual consequence of pouring liquid, specifically the stained ground shown in the fourth row—details entirely missed by the baseline. Additionally, fine-grained interactions in the third row and accumulation dynamics in the second row are faithfully preserved in the reconstructed latent space, verifying that our method retains both temporal logic and spatial semantics.

that is essential for distinguishing "pouring" from merely "holding." This capability extends to fine-grained interactions as well; as illustrated by the "Plugging [something] into [something]" sequence in the third row, our method preserves the precise alignment and insertion phase often lost in strided sampling.

High-Fidelity Spatial Reconstruction. The rightmost column visualizes the decoded output from our optimized latent codes. Despite the significant compression ratio utilizing only about 0.13% of the original raw data size and the inherent dimensionality reduction of the VAE, the reconstructed frames retain rich semantic details. While minor high-frequency textures may be smoothed, the object identities and motion cues remain distinct. This confirms that VideoCompressa learns to store highly discriminative visual features in the latent space rather than relying on adversarial noise or overfitting to background statistics.

8. Conclusion

In this work, we addressed the critical challenge of prohibitive storage and computational costs associated with large-scale video datasets. We introduced VideoCompressa, a novel dataset synthesis framework that reimagines video compression as a principled temporal information selection problem. Our core innovation lies in the synergy between a differentiable Gumbel keyframe selector and a gradientguided latent optimization process. This combination enables the model to automatically identify and leverage the most informative frames into a compact, semantically rich latent representation. The success of VideoCompressa opens several exciting avenues for future research. This perspective on "learning what to ignore" provides a scalable and interpretable foundation for the next generation of video dataset synthesis. We believe this work will inspire further exploration into dynamic, content-aware data compression, with

promising extensions to multimodal learning and the development of large-scale, yet highly efficient, video-language models.

References

- [1] Josh Achiam, Steven Adler, Sandhini Agarwal, Lama Ahmad, Ilge Akkaya, Florencia Leoni Aleman, Diogo Almeida, Janko Altenschmidt, Sam Altman, Shyamal Anadkat, et al. Gpt-4 technical report. arXiv preprint arXiv:2303.08774, 2023. 1
- [2] Anurag Arnab, Mostafa Dehghani, Georg Heigold, Chen Sun, Mario Lučić, and Cordelia Schmid. ViViT: A video vision transformer. In *Proceedings of the IEEE/CVF International Conference on Computer Vision (ICCV)*, pages 6836–6846, 2021. A key paper adapting the Vision Transformer (ViT) architecture specifically for video, showing SOTA performance.
- [3] Milan K Asha Paul, Jeyaraman Kavitha, and P Arockia Jansi Rani. Key-frame extraction techniques: A review. *Recent Patents on Computer Science*, 11(1):3–16, 2018. 2
- [4] Shuai Bai, Keqin Chen, Xuejing Liu, Jialin Wang, Wenbin Ge, Sibo Song, Kai Dang, Peng Wang, Shijie Wang, Jun Tang, Humen Zhong, Yuanzhi Zhu, Mingkun Yang, Zhaohai Li, Jianqiang Wan, Pengfei Wang, Wei Ding, Zheren Fu, Yiheng Xu, Jiabo Ye, Xi Zhang, Tianbao Xie, Zesen Cheng, Hang Zhang, Zhibo Yang, Haiyang Xu, and Junyang Lin. Qwen2.5-vl technical report. arXiv preprint arXiv:2502.13923, 2025.
- [5] Tianyi Bai, Hao Liang, Binwang Wan, Yanran Xu, Xi Li, Shiyu Li, Ling Yang, Bozhou Li, Yifan Wang, Bin Cui, et al. A survey of multimodal large language model from a datacentric perspective. arXiv preprint arXiv:2405.16640, 2024.
- [6] Ollin Boer Bohan. Taesd: Tiny autoencoder for stable diffusion. https://huggingface.co/madebyollin/taesd, 2023. Accessed: 2025-11-09. 2, 5
- [7] Joao Carreira and Andrew Zisserman. Quo vadis, action recognition? a new model and the kinetics dataset. In Pro-

- ceedings of the IEEE Conference on Computer Vision and Pattern Recognition (CVPR), 2017. 4, 5
- [8] George Cazenavette, Tongzhou Wang, Antonio Torralba, Alexei A Efros, and Jun-Yan Zhu. Dataset distillation by matching training trajectories. In *Proceedings of the IEEE/CVF Conference on Computer Vision and Pattern Recognition*, pages 4750–4759, 2022. 1, 5
- [9] George Cazenavette, Tongzhou Wang, Antonio Torralba, Alexei A Efros, and Jun-Yan Zhu. Dataset distillation by matching training trajectories. In *Proceedings of the IEEE/CVF Conference on Computer Vision and Pattern Recognition*, pages 4750–4759, 2022. 1
- [10] Chengliang Chai, Jiayi Wang, Nan Tang, Ye Yuan, Jiabin Liu, Yuhao Deng, and Guoren Wang. Efficient coreset selection with cluster-based methods. In *Proceedings of the* 29th ACM SIGKDD Conference on Knowledge Discovery and Data Mining, pages 167–178, 2023. 2
- [11] Yang Chen, Sheng Guo, Bo Zheng, and Limin Wang. A large-scale study on video action dataset condensation. *arXiv* preprint arXiv:2412.21197, 2024. 1, 2
- [12] Christoph Feichtenhofer, Haoqi Fan, Jitendra Malik, and Kaiming He. Slowfast networks for video recognition. In Proceedings of the IEEE/CVF International Conference on Computer Vision (ICCV), pages 6202–6211, 2019. Directly addresses the computational overhead of video processing by proposing an efficient two-pathway model. 1
- [13] Minggang Gan, Jinting Liu, Yuxuan He, Aobo Chen, and Qianzhao Ma. Keyframe selection via deep reinforcement learning for skeleton-based gesture recognition. *IEEE Robotics and Automation Letters*, 8(11):7807–7814, 2023. 2
- [14] Rohit Girdhar, Joao Carreira, Carl Doersch, and Andrew Zisserman. Video action transformer network. In *Proceedings* of the *IEEE/CVF* conference on computer vision and pattern recognition, pages 244–253, 2019. 2
- [15] Raghav Goyal, Samira Ebrahimi Kahou, Vincent Michalski, Joanna Materzynska, Susanne Westphal, Heuna Kim, Valentin Haenel, Ingo Fruend, Peter Yianilos, Moritz Mueller-Freitag, Florian Hoppe, Christian Thurau, Ingo Bax, and Roland Memisevic. The "something something" video database for learning and evaluating visual common sense. In Proceedings of the IEEE International Conference on Computer Vision (ICCV), 2017. 4
- [16] Chengcheng Guo, Bo Zhao, and Yanbing Bai. Deepcore: A comprehensive library for coreset selection in deep learning. In *International Conference on Database and Expert Systems* Applications, pages 181–195. Springer, 2022. 2
- [17] Ziyao Guo, Kai Wang, George Cazenavette, Hui Li, Kaipeng Zhang, and Yang You. Towards lossless dataset distillation via difficulty-aligned trajectory matching. In *The Twelfth International Conference on Learning Representations*, 2024.
- [18] Kai Hu, Feng Gao, Xiaohan Nie, Peng Zhou, Son Tran, Tal Neiman, Lingyun Wang, Mubarak Shah, Raffay Hamid, Bing Yin, et al. M-llm based video frame selection for efficient video understanding. In *Proceedings of the Computer Vision* and Pattern Recognition Conference, pages 13702–13712, 2025. 2

- [19] De-An Huang, Vignesh Ramanathan, Dhruv Mahajan, Lorenzo Torresani, Manohar Paluri, Li Fei-Fei, and Juan Carlos Niebles. What makes a video a video: Analyzing temporal information in video understanding models and datasets. In Proceedings of the IEEE Conference on Computer Vision and Pattern Recognition, pages 7366–7375, 2018. 1, 2
- [20] Iris AM Huijben, Wouter Kool, Max B Paulus, and Ruud JG Van Sloun. A review of the gumbel-max trick and its extensions for discrete stochasticity in machine learning. *IEEE transactions on pattern analysis and machine intelligence*, 45 (2):1353–1371, 2022. 2
- [21] Matthew S Hutchinson and Vijay N Gadepally. Video action understanding. *IEEE Access*, 9:134611–134637, 2021. 2
- [22] Eric Jang, Shixiang Gu, and Ben Poole. Categorical reparameterization with gumbel-softmax. *arXiv preprint arXiv:1611.01144*, 2016. 2, 4
- [23] Will Kay, Joao Carreira, Karen Simonyan, Andrew Zisserman, et al. The kinetics human action video dataset. In *Proceedings of the 2017 ACM SIGKDD International Conference on Knowledge Discovery and Data Mining*, 2017. Foundational large-scale video dataset (Kinetics-400) that spurred video understanding research. 1, 2
- [24] Lingdong Kong, Xiang Xu, Jiawei Ren, Wenwei Zhang, Liang Pan, Kai Chen, Wei Tsang Ooi, and Ziwei Liu. Multimodal data-efficient 3d scene understanding for autonomous driving. *IEEE Transactions on Pattern Analysis and Machine Intelligence*, 2025. 1
- [25] Hildegard Kuehne, Hueihan Jhuang, Estíbaliz Garrote, Tomaso Poggio, and Thomas Serre. Hmdb: a large video database for human motion recognition. In 2011 International conference on computer vision, pages 2556–2563. IEEE, 2011. 4, 5
- [26] Annie Lang. Defining audio/video redundancy from a limitedcapacity information processing perspective. *Communication research*, 22(1):86–115, 1995.
- [27] Hojun Lee, Suyoung Kim, Junhoo Lee, Jaeyoung Yoo, and Nojun Kwak. Coreset selection for object detection. In Proceedings of the IEEE/CVF Conference on Computer Vision and Pattern Recognition, pages 7682–7691, 2024. 2
- [28] Shiye Lei and Dacheng Tao. A comprehensive survey of dataset distillation. *IEEE Transactions on Pattern Analysis* and Machine Intelligence, 46(1):17–32, 2023. 1, 2
- [29] Hongcheng Li, Yucan Zhou, Xiaoyan Gu, Bo Li, and Weiping Wang. Diversity-enhanced distribution alignment for dataset distillation. In *Proceedings of the IEEE/CVF International* Conference on Computer Vision (ICCV), pages 3747–3756, 2025. 8
- [30] Ning Li, Antai Andy Liu, Jingran Zhang, and Justin Cui. Latent video dataset distillation. arXiv preprint arXiv:2504.17132, 2025. 2
- [31] Ning Li, Antai Andy Liu, Jingran Zhang, and Justin Cui. Latent video dataset distillation. In *Proceedings of the IEEE/CVF Conference on Computer Vision and Pattern Recognition (CVPR), Workshop*, 2025. 5
- [32] Bin Lin, Yang Ye, Bin Zhu, Jiaxi Cui, Munan Ning, Peng Jin, and Li Yuan. Video-llava: Learning united visual representation by alignment before projection. In *Proceedings of the*

- 2024 Conference on Empirical Methods in Natural Language Processing, pages 5971–5984, 2024. 2
- [33] Ji Lin, Chuang Gan, and Song Han. Tsm: Temporal shift module for efficient video understanding. In *Proceedings of* the IEEE/CVF international conference on computer vision, pages 7083–7093, 2019. 1
- [34] Xuyang Liu, Yiyu Wang, Junpeng Ma, and Linfeng Zhang. Video compression commander: Plug-and-play inference acceleration for video large language models. *arXiv preprint* arXiv:2505.14454, 2025. 2
- [35] Xuyang Liu, Zichen Wen, Shaobo Wang, Junjie Chen, Zhishan Tao, Yubo Wang, Xiangqi Jin, Chang Zou, Yiyu Wang, Chenfei Liao, et al. Shifting ai efficiency from model-centric to data-centric compression. arXiv preprint arXiv:2505.19147, 2025. 2
- [36] Leland McInnes, John Healy, Nathaniel Saul, and Lukas Grossberger. Umap: Uniform manifold approximation and projection. *The Journal of Open Source Software*, 3(29):861, 2018. 8
- [37] Yue Min, Shaobo Wang, Jiaze Li, Tianle Niu, Junxin Fan, Yongliang Miao, Lijin Yang, and Linfeng Zhang. Imagebinddc: Compressing multi-modal data with imagebind-based condensation. Proceedings of the AAAI Conference on Artificial Intelligence, 2026. 1
- [38] Clinton Mo, Kun Hu, Shaohui Mei, Zebin Chen, and Zhiyong Wang. Keyframe extraction from motion capture sequences with graph based deep reinforcement learning. In *Proceedings* of the 29th ACM International Conference on Multimedia, pages 5194–5202, 2021. 2
- [39] Brian B Moser, Arundhati S Shanbhag, Stanislav Frolov, Federico Raue, Joachim Folz, and Andreas Dengel. A coreset selection of coreset selection literature: Introduction and recent advances. arXiv preprint arXiv:2505.17799, 2025. 2
- [40] Saralees Nadarajah and Samuel Kotz. The beta gumbel distribution. *Mathematical Problems in engineering*, 2004(4): 323–332, 2004.
- [41] Mansheej Paul, Surya Ganguli, and Gintare Karolina Dziugaite. Deep learning on a data diet: Finding important examples early in training. *Advances in neural information processing systems*, 34:20596–20607, 2021. 5, 7
- [42] Elham Ravanbakhsh, Yongqing Liang, J Ramanujam, and Xin Li. Deep video representation learning: a survey. *Multimedia Tools and Applications*, 83(20):59195–59225, 2024. 1
- [43] Ahmad Sajedi, Samir Khaki, Ehsan Amjadian, Lucy Z Liu, Yuri A Lawryshyn, and Konstantinos N Plataniotis. Datadam: Efficient dataset distillation with attention matching. In *Proceedings of the IEEE/CVF International Conference on Computer Vision*, pages 17097–17107, 2023. 1, 2
- [44] Ahmad Sajedi, Samir Khaki, Lucy Z Liu, Ehsan Amjadian, Yuri A Lawryshyn, and Konstantinos N Plataniotis. Datato-model distillation: Data-efficient learning framework. In European Conference on Computer Vision, pages 438–457. Springer, 2024. 1
- [45] Yan Shu, Zheng Liu, Peitian Zhang, Minghao Qin, Junjie Zhou, Zhengyang Liang, Tiejun Huang, and Bo Zhao. Videoxl: Extra-long vision language model for hour-scale video understanding. In *Proceedings of the Computer Vision and*

- Pattern Recognition Conference, pages 26160–26169, 2025.
- [46] Alaia Solko-Breslin, Seewon Choi, Ziyang Li, Neelay Velingker, Rajeev Alur, Mayur Naik, and Eric Wong. Data-efficient learning with neural programs. *Advances in Neural Information Processing Systems*, 37:14666–14689, 2024. 1
- [47] Khurram Soomro, Amir Roshan Zamir, and Mubarak Shah. Ucf101: A dataset of 101 human actions classes from videos in the wild. 2012. 4
- [48] Ben Sorscher, Robert Geirhos, Shashank Shekhar, Surya Ganguli, and Ari Morcos. Beyond neural scaling laws: beating power law scaling via data pruning. Advances in Neural Information Processing Systems, 35:19523–19536, 2022.
- [49] Peng Sun, Bei Shi, Daiwei Yu, and Tao Lin. On the diversity and realism of distilled dataset: An efficient dataset distillation paradigm. In *Proceedings of the IEEE/CVF Conference* on Computer Vision and Pattern Recognition, pages 9390– 9399, 2024. 1, 2
- [50] Xi Tang, Jihao Qiu, Lingxi Xie, Yunjie Tian, Jianbin Jiao, and Qixiang Ye. Adaptive keyframe sampling for long video understanding. In *Proceedings of the Computer Vision and Pattern Recognition Conference*, pages 29118–29128, 2025.
- [51] Yunlong Tang, Jing Bi, Siting Xu, Luchuan Song, Susan Liang, Teng Wang, Daoan Zhang, Jie An, Jingyang Lin, Rongyi Zhu, et al. Video understanding with large language models: A survey. *IEEE Transactions on Circuits and Systems* for Video Technology, 2025. 1
- [52] Mariya Toneva, Alessandro Sordoni, Remi Tachet des Combes, Adam Trischler, Yoshua Bengio, and Geoffrey J Gordon. An empirical study of example forgetting during deep neural network learning. arXiv preprint arXiv:1812.05159, 2018. 5, 7
- [53] Zhan Tong, Yibing Song, Jue Wang, and Limin Wang. Video-MAE: Masked autoencoders are data-efficient learners for self-supervised video pre-training. In Advances in Neural Information Processing Systems (NeurIPS), pages 10078–10093, 2022. A highly influential and state-of-the-art self-supervised learning method for video understanding. 1, 2
- [54] Shaobo Wang, Yicun Yang, Zhiyuan Liu, Chenghao Sun, Xuming Hu, Conghui He, and Linfeng Zhang. Dataset distillation with neural characteristic function: A minmax perspective. In *Proceedings of the Computer Vision and Pattern Recognition Conference*, pages 25570–25580, 2025. 1, 2
- [55] Shaobo Wang, Yantai Yang, Qilong Wang, Kaixin Li, Linfeng Zhang, and Junchi Yan. Not all samples should be utilized equally: Towards understanding and improving dataset distillation. Synthetic Data for Computer Vision Workshop at CVPR, 2025.
- [56] Shaobo Wang, Yantai Yang, Shuaiyu Zhang, Chenghao Sun, Weiya Li, Xuming Hu, and Linfeng Zhang. DRUPI: Dataset reduction using privileged information. In *The Future of Machine Learning Data Practices and Repositories at ICLR* 2025, 2025.
- [57] Tongzhou Wang, Jun-Yan Zhu, Antonio Torralba, and Alexei A Efros. Dataset distillation. arXiv preprint arXiv:1811.10959, 2018. 1, 2

- [58] Yi Wang, Kunchang Li, Xinhao Li, Jiashuo Yu, Yinan He, Guo Chen, Baoqi Pei, Rongkun Zheng, Zun Wang, Yansong Shi, et al. Internvideo2: Scaling foundation models for multimodal video understanding. In *European Conference on Computer Vision*, pages 396–416. Springer, 2024. 1
- [59] Ziyu Wang, Yue Xu, Cewu Lu, and Yong-Lu Li. Dancing with still images: Video distillation via static-dynamic disentanglement. arXiv preprint arXiv:2312.00362, 2023. 1, 2
- [60] Ziyu Wang, Yue Xu, Cewu Lu, and Yong-Lu Li. Dancing with still images: Video distillation via static-dynamic disentanglement. In Proceedings of the IEEE/CVF Conference on Computer Vision and Pattern Recognition (CVPR), pages 23307–23316, 2024. 5
- [61] Max Welling. Herding dynamical weights to learn. In *Proceedings of the 26th annual international conference on machine learning*, pages 1121–1128, 2009. 5, 7
- [62] Wayne Wolf. Key frame selection by motion analysis. In 1996 IEEE international conference on acoustics, speech, and signal processing conference proceedings, pages 1228–1231. IEEE, 1996. 2
- [63] Chenfei Wu, Jiahao Li, Jingren Zhou, Junyang Lin, Kaiyuan Gao, Kun Yan, Sheng-ming Yin, Shuai Bai, Xiao Xu, Yilei Chen, et al. Qwen-image technical report. arXiv preprint arXiv:2508.02324, 2025. 1
- [64] Furui Xu, Shaobo Wang, Luo Zhongwei, and Linfeng Zhang. Rethinking dataset pruning from a generalization perspective. In *The Future of Machine Learning Data Practices and Repositories at ICLR* 2025, 2025.
- [65] Lei Yan, Jiaxiong Weng, Daobo Ma, et al. Enhanced transformer-based algorithm for key-frame action recognition in basketball shooting. 2025. 2
- [66] Jinhui Ye, Zihan Wang, Haosen Sun, Keshigeyan Chandrasegaran, Zane Durante, Cristobal Eyzaguirre, Yonatan Bisk, Juan Carlos Niebles, Ehsan Adeli, Li Fei-Fei, et al. Rethinking temporal search for long-form video understanding. In Proceedings of the Computer Vision and Pattern Recognition Conference, pages 8579–8591, 2025.
- [67] Ruonan Yu, Songhua Liu, and Xinchao Wang. Dataset distillation: A comprehensive review. *IEEE transactions on pattern analysis and machine intelligence*, 46(1):150–170, 2023.
- [68] Hang Zhang, Xin Li, and Lidong Bing. Video-llama: An instruction-tuned audio-visual language model for video understanding. arXiv preprint arXiv:2306.02858, 2023. 2
- [69] Qiyuan Zhang, Fuyuan Lyu, Zexu Sun, Lei Wang, Weixu Zhang, Wenyue Hua, Haolun Wu, Zhihan Guo, Yufei Wang, Niklas Muennighoff, et al. A survey on test-time scaling in large language models: What, how, where, and how well? arXiv preprint arXiv:2503.24235, 2025.
- [70] Bo Zhao and Hakan Bilen. Dataset condensation with distribution matching, 2022. 1, 5
- [71] Yinjie Zhao, Heng Zhao, Bihan Wen, Yew-Soon Ong, and Joey Tianyi Zhou. Video set distillation: Information diversification and temporal densification. *arXiv preprint arXiv:2412.00111*, 2024. 1, 2

VideoCompressa: Data-Efficient Video Understanding via Joint Temporal Compression and Spatial Reconstruction

Supplementary Material

9. Theorm of Gumbel-Based Selection

This section provides the theoretical foundation for our differentiable keyframe selection mechanism. We first provide a formal proof for the Gumbel-Max trick (Theorem 1), demonstrating that adding i.i.d. Gumbel noise to logits and taking the index of the maximum element is equivalent to sampling from the categorical distribution. Subsequently, we analyze the gradient approximation (Theorem 2), showing that the gradients derived from our Gumbel-Softmax relaxation serve as a bounded approximation to the gradients of the discrete Straight-Through Estimator, thereby justifying the consistency of our end-to-end training strategy.

Theorem 1 (The Gumbel-Max Trick). Let q_1, \ldots, q_K be a set of logits. Let g_1, \ldots, g_K be i.i.d. random variables from the standard Gumbel distribution. Then:

$$P\left(j = \arg\max_{i} (q_i + g_i)\right) = \frac{\exp(q_j)}{\sum_{i=1}^{K} \exp(q_i)}$$

Proof. The standard Gumbel distribution is defined by its CDF, $F(x) = \exp(-\exp(-x))$, and its PDF, $f(x) = \exp(-x - \exp(-x))$.

Let $k = \arg \max_i (q_i + g_i)$. The event k = j occurs if and only if $q_j + g_j$ is greater than all other $q_i + g_i$ for $i \neq j$. We compute this probability by integrating over all possible values of g_j . Let $g_j = x$:

$$P(k = j) = P(q_j + g_j \ge q_i + g_i, \ \forall i \ne j)$$
$$= \int_{-\infty}^{\infty} P(g_i \le x + q_j - q_i, \ \forall i \ne j) f(x) dx$$

Since the g_i are i.i.d., the joint probability inside the integral can be factored into a product of individual CDFs:

$$P(k=j) = \int_{-\infty}^{\infty} \left(\prod_{i \neq j} F(x + q_j - q_i) \right) f(x) dx$$
$$= \int_{-\infty}^{\infty} \left(\prod_{i \neq j} \exp(-\exp(-(x + q_j - q_i))) \right)$$
$$\cdot \exp(-x - \exp(-x)) dx$$

The product of exponentials can be rewritten as the exponential of a sum. This is the step where we break the long

equation for a two-column layout.

$$P(k = j) = \int_{-\infty}^{\infty} \exp\left(-\sum_{i \neq j} \exp(-(x + q_j - q_i))\right)$$

$$\cdot \exp(-x) \exp(-\exp(-x)) dx$$

$$= \int_{-\infty}^{\infty} \exp(-x) \exp(-\exp(-x))$$

$$\cdot \left[1 + \sum_{i \neq j} \exp(q_i - q_j)\right] dx$$

The term in the brackets can be simplified by noting that $1 = \exp(q_i - q_i)$:

$$1 + \sum_{i \neq j} \exp(q_i - q_j) = \sum_{i=1}^K \exp(q_i - q_j)$$

Let $C = \sum_{i=1}^{K} \exp(q_i - q_j)$. This constant is independent of x. The integral simplifies to:

$$P(k=j) = \int_{-\infty}^{\infty} \exp(-x) \exp(-C \cdot \exp(-x)) dx$$

We solve this using the substitution $u=C\cdot\exp(-x)$. This gives $du=-C\cdot\exp(-x)dx$, so $\exp(-x)dx=-\frac{1}{C}du$. The integration limits change from $(-\infty,\infty)$ for x to $(\infty,0)$ for y

$$P(k=j) = \int_{\infty}^{0} \exp(-u) \left(-\frac{1}{C}\right) du$$
$$= \frac{1}{C} \int_{0}^{\infty} \exp(-u) du = \frac{1}{C} [-\exp(-u)]_{0}^{\infty}$$
$$= \frac{1}{C} (0 - (-1)) = \frac{1}{C}$$

Substituting the definition of C back, we get:

$$P(k = j) = \frac{1}{\sum_{i=1}^{K} \exp(q_i - q_j)}$$

$$= \frac{\exp(q_j)}{\exp(q_j) \sum_{i=1}^{K} \exp(q_i - q_j)}$$

$$= \frac{\exp(q_j)}{\sum_{i=1}^{K} \exp(q_i)}$$

This is the softmax probability of the j-th category, which completes the proof.

Theorem 2 (Gradient Approximation Bound). Let q be the logit vector and g be the Gumbel noise vector. We define the hard selection vector \mathbf{y}^h via Gumbel-Max and the soft selection vector \mathbf{y}^s (via Gumbel-Softmax with temperature τ) as:

$$\mathbf{y}^h = one_hot\left(rg \max(\mathbf{q} + \mathbf{g})\right), \quad \mathbf{y}^s = softmax\left(rac{\mathbf{q} + \mathbf{g}}{ au}
ight)$$

Assume the downstream loss function \mathcal{L} is L-Lipschitz smooth with respect to the selection weights. The error between the gradient of our method (\mathbf{g}_{GS}) and the Straight-Through Estimator gradient (\mathbf{g}_{ST}) is bounded by a linear function of τ :

$$\|\mathbf{g}_{GS} - \mathbf{g}_{ST}\| \le C \cdot \tau$$

where C is a constant independent of τ .

Proof. The two gradients with respect to the scorer parameters ϕ are defined as:

$$\mathbf{g}_{GS} = \nabla_{\phi} \mathcal{L}(\mathbf{y}^s) = \frac{\partial \mathcal{L}}{\partial \mathbf{y}^s} \frac{\partial \mathbf{y}^s}{\partial \mathbf{q}} \frac{\partial \mathbf{q}}{\partial \phi}$$
(9)

$$\mathbf{g}_{ST} = \nabla_{\phi}^{STE} \mathcal{L} \approx \frac{\partial \mathcal{L}}{\partial \mathbf{y}^{h}} \frac{\partial \mathbf{y}^{s}}{\partial \mathbf{q}} \frac{\partial \mathbf{q}}{\partial \phi}$$
(10)

Note that STE uses the hard sample y^h for the forward pass (loss computation) but approximates the backward pass using the soft Jacobian $\frac{\partial y^s}{\partial \mathbf{q}}$. The difference in gradients is:

$$\|\mathbf{g}_{GS} - \mathbf{g}_{ST}\| = \left\| \left(\frac{\partial \mathcal{L}}{\partial \mathbf{v}^s} - \frac{\partial \mathcal{L}}{\partial \mathbf{v}^h} \right) \frac{\partial \mathbf{y}^s}{\partial \mathbf{q}} \frac{\partial \mathbf{q}}{\partial \phi} \right\|$$

Using the Cauchy-Schwarz inequality and the sub-multiplicativity of norms:

$$\|\mathbf{g}_{GS} - \mathbf{g}_{ST}\| \le \left\| \frac{\partial \mathcal{L}}{\partial \mathbf{y}^s} - \frac{\partial \mathcal{L}}{\partial \mathbf{y}^h} \right\| \cdot \left\| \frac{\partial \mathbf{y}^s}{\partial \mathbf{q}} \frac{\partial \mathbf{q}}{\partial \phi} \right\|$$

By the *L*-Lipschitz smoothness assumption of \mathcal{L} , the first term is bounded by the distance between the soft and hard samples:

$$\left\| \frac{\partial \mathcal{L}}{\partial \mathbf{y}^s} - \frac{\partial \mathcal{L}}{\partial \mathbf{y}^h} \right\| \le L \|\mathbf{y}^s - \mathbf{y}^h\|$$

It is a known property of the Softmax function that $\mathbf{y}^s(\tau)$ converges to \mathbf{y}^h as $\tau \to 0$. Specifically, for a fixed set of distinct logits, the approximation error is bounded by $\mathcal{O}(\tau)$. Thus, there exists a constant C_1 such that $\|\mathbf{y}^s - \mathbf{y}^h\| \le C_1 \tau$.

Thus, there exists a constant C_1 such that $\|\mathbf{y}^s - \mathbf{y}^h\| \le C_1 \tau$. Let $C_2 = \sup \|\frac{\partial \mathbf{y}^s}{\partial \mathbf{q}} \frac{\partial \mathbf{q}}{\partial \phi}\|$ be the upper bound of the gradient magnitude, which is finite in practice due to bounded activations and weights. Combining these inequalities:

$$\|\mathbf{g}_{GS} - \mathbf{g}_{ST}\| \le (L \cdot C_1 \cdot \tau) \cdot C_2 = (LC_1C_2) \cdot \tau$$

Setting $C = LC_1C_2$, we obtain $\|\mathbf{g}_{GS} - \mathbf{g}_{ST}\| \le C \cdot \tau$. \square

10. Pseudo Code of VideoCompressa

Our method, VideoCompressa, reframes video data synthesis as a dynamic latent compression problem for data-efficient video understanding. As shown in the Algorithm 1, the algorithm consists of three stages. In the Latent Code Initialization stage, each video frame in the real dataset is encoded into a compact latent representation using a pretrained and frozen VAE, shifting optimization from pixel space to a structured latent space. In the Joint Optimization stage, we jointly train the latent codes, a frame scorer, and a video understanding network. Latent codes are decoded, scored, and softly sampled via the Gumbel-Softmax trick, which enables gradients from the classification loss to update all components end-to-end, including the selected latent codes. In the Deterministic Keyframe Extraction stage, the trained scorer selects the top-K most informative frames for each video. The corresponding optimized latent codes form the final compressed synthetic dataset, which is significantly smaller than the original data but highly informative for downstream tasks.

11. Implementation Details

Latent Code Initialization. To initialize the latent representations, we employed a pre-trained Taesd-VAE encoder. All video frames were processed in batches of 8. To ensure a compact latent space, the VAE was configured with channel pruning on 30% of its parameters and Tucker/PCA compression at a ratio of 0.75, which further reduced the dimensionality of the initial latent codes.

Frame Scorer and Gumbel-Softmax Parameters. The frame scorer is a lightweight convolutional network designed to produce a scalar importance logit for each frame. In our experiments, this module consisted of two 3×3 convolutional layers followed by a linear projection layer. For end-to-end training, we utilized the Gumbel-Softmax technique to enable differentiable sampling of keyframes. The Gumbel-Softmax distribution was controlled by a temperature parameter set to $\tau=1.0$. The frame scorer network was optimized using an Adam optimizer with a learning rate of 1×10^{-3} .

Synthetic Latent Code Optimization. The synthetic latent codes were optimized jointly with the frame scorer and the downstream video understanding network, guided solely by the cross-entropy classification loss. During each training iteration, the latent codes were updated for 4 optimization steps using a batch size of 64. We used an Adam optimizer with a learning rate of 1×10^{-2} for this process.

Evaluation of the synthesized dataset. To assess the quality of the synthesized dataset, we trained a new instance of the video understanding network from scratch using the distilled latent representations. This network was trained for 100 epochs using Stochastic Gradient Descent (SGD).

Algorithm 1 VideoCompressa: Joint Temporal Compression and Spatial Reconstruction

```
Input: Real dataset \mathcal{D}_{\text{train}} = \{(V_i, y_i)\}_{i=1}^N, pretrained
VAE (\mathcal{E}, \psi), number of keyframes K, random initialized
Frame scorer \phi, Understanding network \mathcal{M}_{\theta}.
Learnable Variables: Latent codes \{Z_i\}, scorer parame-
ters \phi, Understanding network parameters \theta.
// Stage 1: Latent Code Initialization
for each video V_i = \{f_{i,t}\}_{t=1}^{T_i} in \mathcal{D}_{\text{train}} do
       Z_i \leftarrow \{\mathcal{E}(f_{i,t})\}
// Stage 2: Gumbel-Based Temporal Compression
while not converged do
       Sample mini-batch \mathcal{B}.
       for each i \in \mathcal{B} do
             \hat{V}_i = \{\psi(z_{i,t})\}_{t=1}^{T_i}
             q_i = \phi(\hat{V}_i) for k = 1, \dots, K do
            Sample Gumbel noise g_i^{(k)} p_i^{(k)} \leftarrow \operatorname{Softmax} \left( (q_i + g_i^{(k)}) / \tau \right) \tilde{f}_i^{(k)} \leftarrow \sum_{t=1}^{T_i} p_{i,t}^{(k)} \hat{f}_{i,t} end for
            \tilde{V}_i \leftarrow \{\tilde{f}_i^{(k)}\}_{k=1}^K
\hat{y}_i = \mathcal{M}_{\theta}(\tilde{V}_i)
       end for
      Compute loss \mathcal{L} = \frac{1}{|\mathcal{B}|} \sum_{i \in \mathcal{B}} \mathrm{CE}(\hat{y}_i, y_i)
       Update \{Z_i\}, \phi, \theta using gradients from \mathcal{L}
end while
// Stage 3: Latent Spatial Reconstruction
for each video i do
      \hat{V}_i = \{\psi(z_{i,t})\}_{t=1}^{T_i}
q_i = \phi(\hat{V}_i)
T_i^K \leftarrow \text{top-K}(q_i)
Z_i^* \leftarrow \{z_{i,t}\}_{t \in T_i^K}
Output: Synthetic latent dataset S^* = \{Z_i^*\}_{i=1}^N.
```

The training hyperparameters were set as follows: a learning rate of 0.01, a batch size of 256, a momentum of 0.9, and a weight decay of 5×10^{-4} .

12. More Experiments of Sensitivity Analysis

To investigate the impact of the number of distillation steps on our method's performance, we conducted a sensitivity analysis on the HMDB51 and UCF101 datasets. Table 6 presents the classification accuracy as a function of the number of optimization steps, where all experiments utilize the Gumbel-Max key-frame selector with a 4-frame budget.

The results clearly demonstrate that our framework converges remarkably fast. A significant performance gain is

Table 6. Sensitivity analysis of the number of distillation steps on the HMDB51 and UCF101 datasets. The results demonstrate that our method converges rapidly, achieving a significant performance gain after the first step and peaking after four steps. For this analysis, all configurations use the Gumbel-Max key-frame selector with a 4-frame budget.

Training step	0	1	2	4	8
			26.47 ± 0.46 27.81 ± 0.46		

achieved after just the first distillation step for both datasets. The accuracy continues to improve and peaks at four steps, reaching 27.78% on HMDB51 and 29.84% on UCF101. Interestingly, extending the process to eight steps leads to a slight degradation in performance, suggesting that four steps are sufficient to achieve optimal results while avoiding potential overfitting to the guiding network. This rapid convergence underscores the efficiency of our joint optimization strategy in learning a compact and effective data representation.